


Isoelectronic tuning of heavy fermion systems: Proposal to synthesize $\text{Ce}_3\text{Sb}_4\text{Pd}_3$

Jan M. Tomczak *

Institute of Solid State Physics, Vienna University of Technology, A-1040 Vienna, Austria

 (Received 30 July 2019; revised manuscript received 12 December 2019; published 13 January 2020)

The study of (quantum) phase transitions in heavy fermion compounds relies on a detailed understanding of the microscopic control parameters that induce them. While the influence of external pressure is rather straightforward, atomic substitutions are more involved. Nonetheless, replacing an elemental constituent of a compound with an isovalent atom is, effects of disorder aside, often viewed as merely affecting the lattice constant. Based on this picture of chemical pressure, the unit-cell volume is identified as an empirical proxy for the Kondo coupling. Here, instead, we propose an “orbital scenario” in which the coupling in complex systems can be tuned by isoelectronic substitutions with little or no effect onto cohesive properties. Starting with the Kondo insulator $\text{Ce}_3\text{Bi}_4\text{Pt}_3$, we consider, within band theory, isoelectronic substitutions of the pnictogen ($\text{Bi} \rightarrow \text{Sb}$) and/or the precious metal ($\text{Pt} \rightarrow \text{Pd}$). We show for the *isovolume* series $\text{Ce}_3\text{Bi}_4(\text{Pt}_{1-x}\text{Pd}_x)_3$ that the Kondo coupling is in fact substantially modified by the different *radial extent* of the $5d$ (Pt) and $4d$ (Pd) orbitals, while spin-orbit coupling mediated changes are minute. Combining experimental Kondo temperatures with simulated hybridization functions, we also predict effective masses m^* , finding excellent agreement with many-body results for $\text{Ce}_3\text{Bi}_4\text{Pt}_3$. Our analysis motivates studying the so-far unknown Kondo insulator $\text{Ce}_3\text{Sb}_4\text{Pd}_3$, for which we predict $m^*/m_{\text{band}} = O(10)$.

DOI: [10.1103/PhysRevB.101.035116](https://doi.org/10.1103/PhysRevB.101.035116)

I. INTRODUCTION

The physics of materials with f electrons is determined by a delicate interplay of energy scales. The competition between the latter can be tuned by various means, including external fields, pressure, carrier doping, resulting in enormously rich phase diagrams [1–4]. Of particular interest are stimuli that control the (Kondo) coupling strength while leaving (nominal) valence states inert. In the case of heavy fermion metals this allows, for instance, to directly explore Doniach’s phase diagram [5]. Isoelectronic tuning can be achieved, e.g., through external or chemical pressure. In the latter case, elemental constituents are (at least partially) replaced with atoms having the same valence configuration but a different principal quantum number n .

In *binary* compounds, such isoelectronic substitutions directly control the unit-cell volume, as n typically correlates with the element’s bonding radius. Furthermore, calculations of the hybridization of the f states with their surrounding display, in binary compounds, an empirical one-to-one correspondence to the experimental Kondo temperature [6]. Hence, the notion that, both, external and chemical pressure manipulate the Kondo coupling J_K primarily through the change in lattice constants.

For more complex Kondo systems, ternary compounds and above, we here demonstrate that the unit-cell volume (perhaps unsurprisingly) is *not* a good proxy for the size of the Kondo coupling. Consider that in isoelectronic substitutions both the shape and the radial extent of the wave function are different as the principal quantum number changes. This will

affect the hybridization and bonding not just with the atoms hosting the $4f$ orbitals, but also between all other atoms. Therefore, it is not *a priori* clear whether isovalent interperiod

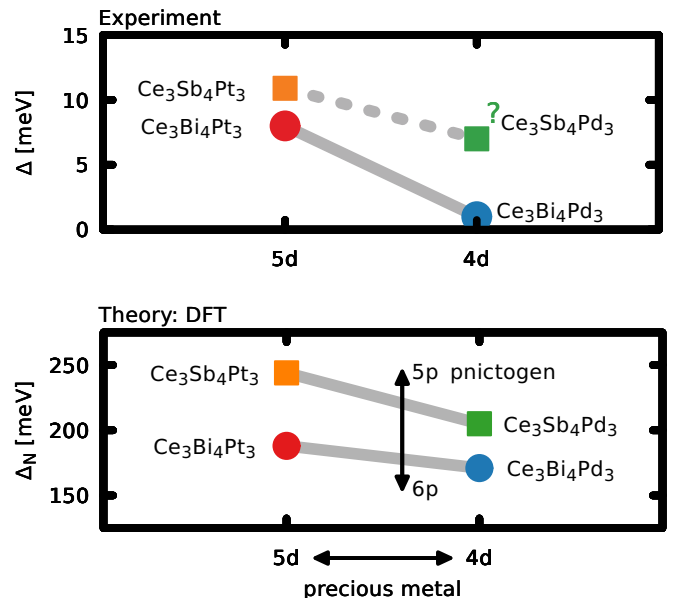


FIG. 1. Trends in the charge gap. Top: experimental gaps of our focus compounds (see also Fig. 2); the value for $\text{Ce}_3\text{Sb}_4\text{Pd}_3$ is unknown. Bottom: theoretical gaps within band theory. Arrows indicate trends for pnictogen ($\text{Bi} \leftrightarrow \text{Sb}$) and precious-metal ($\text{Pt} \leftrightarrow \text{Pd}$) substitution. We seek to identify the microscopic control parameters that these substitutions engage. Replacing the precious metal was shown [7–9] (is predicted, see Sec. IV A) to be isovolume for the Bi (Sb) compounds. Note that the gap Δ_N is measured from the Fermi level to the N point, for reasons explained in the text.

*tomczak.jm@gmail.com

substitutions modify (i) cohesive properties (largely dominated by hybridizations not involving the f orbitals), (ii) the Kondo coupling J_K (controlled by the hybridization of the f electrons with their surrounding), or (iii) both of them.

Here, we explore how isoelectronic tuning affects the itinerancy of f electrons in the family of Kondo insulators [4,10,11] $Ce_3A_4M_3$ ($A = Bi, Sb, M = Pt, Pd$), which is of high current interest [4,12–18]. We consider both possible isovalent substitutions, that of the pnictogen and that of the precious metal, and investigate the detailed interplay of volume, orbital extent, and hybridizations onto the charge gap within band theory. In other words, we elucidate the microscopic parameters that tune $Ce_3A_4M_3$ ($A = Bi, Sb, M = Pt, Pd$) along the arrows in Fig. 1 (bottom).

We find that the difference between the Bi- and the Sb-derived materials are mainly driven by the unit-cell volume, a conventional case of isoelectronic tuning. For the isovolume substitution of the precious metal [7–9] we instead quantify an orbital scenario [4], in which the different *radial extent* of the 5d (Pt) and 4d (Pd) orbitals tunes the Kondo coupling.

Finally, by combining insights from band theory with experimental magnetic susceptibilities, we estimate mass renormalizations (Table I): We find (i) excellent agreement with recent many-body simulations for $Ce_3Bi_4Pt_3$ [14]; (ii) the Pd-based systems have significantly larger renormalizations than the Pt ones; (iii) the Sb members have larger Kondo scales than their Bi counterparts. The latter highly motivates synthesizing and characterizing the so far unknown compound $Ce_3Sb_4Pd_3$ as well as the series $Ce_3Sb_4(Pt_{1-x}Pd_x)_3$, in which the isovalent substitution can be studied at more accessible conditions than for the Bi series.

II. SURVEY OF EXPERIMENTAL RESULTS AND PREVIOUS INTERPRETATIONS

We summarize pertinent experimental findings and their interpretation for the materials under consideration (for a broader perspective see Refs. [4,11]): As seen in the collection of resistivities (top) and magnetic susceptibilities (bottom) in Fig. 2, the charge and spin gap, Δ and Δ_s , and the crossover temperature T_χ^{\max} indicative of the onset of Kondo screening, vary significantly in these materials: Interchanging of pnictogen and/or precious-metal elements markedly tunes the energy scales. The tendencies of the charge gap Δ , on which we will focus our attention, are condensed in Fig. 1 (top): The Pt-based compounds are prime examples of Kondo insulators [7,10,11,19–21], with the Sb member having a slightly larger charge gap than its Bi counterpart. Exchanging Pt with Pd in $Ce_3Bi_4Pt_3$ diminishes the charge gap [7,22], while the volume remains constant [7–9]. The isovolume nature of the precious-metal substitution was recently confirmed by studying the continuous series $Ce_3Bi_4(Pt_{1-x}Pd_x)_3$ [12]. The end member $Ce_3Bi_4Pd_3$ [9] has been characterized as a semimetal [12], while more recent experiments [17] extract a gap $\Delta \sim 2$ meV from the Hall resistivity and the critical magnetic field. Under the assumption of a direct correspondence between unit-cell volume and the Kondo coupling J_K , it was initially asserted [12] that J_K is independent of x in isovolume $Ce_3Bi_4(Pt_{1-x}Pd_x)_3$. It was then concluded [12]

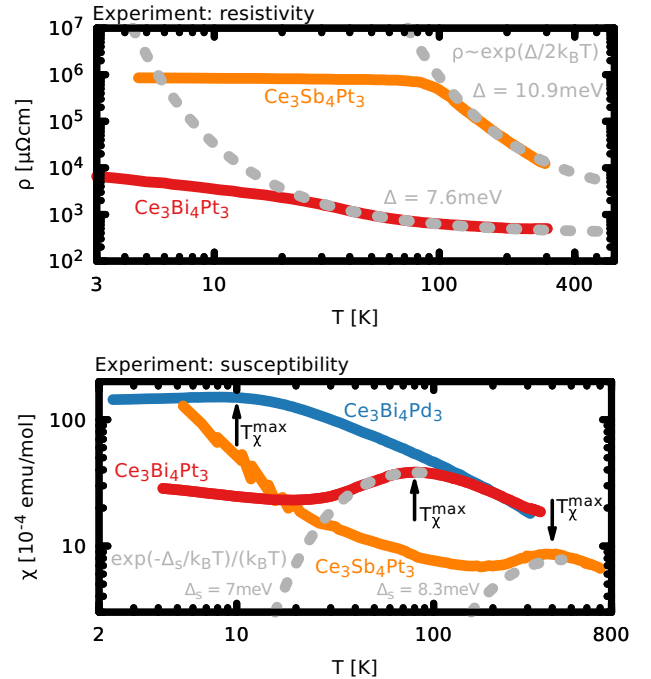


FIG. 2. Survey of experimental data. Shown are the resistivities from Refs. [21,22] (top panel) and magnetic susceptibilities from Refs. [7,20] (bottom panel) of $Ce_3Bi_4Pt_3$ and $Ce_3Sb_4Pt_3$, respectively. The susceptibility of $Ce_3Bi_4Pd_3$ is from Ref. [12]. Using phenomenological fits as indicated (in gray, see also Ref. [4]), the charge and spin gaps are extracted. For χ , the fitting ignores low-temperature Curie-Weiss contributions likely to derive from impurities. The gap in $Ce_3Bi_4Pd_3$ (no data shown) has been estimated as ~ 2 meV [17].

that the decrease of energy scales with increasing x is driven by the change in the spin-orbit coupling, owing to the mass differences of Pt and Pd, an exciting perspective in view of the recent proposals of topological Kondo insulators [23,24]. Here, instead, we argue in favor of a substantial evolution of the Kondo coupling in the series $Ce_3Bi_4(Pt_{1-x}Pd_x)_3$. The compound $Ce_3Sb_4Pd_3$ has, to the best of our knowledge, not yet been synthesized.

III. CRYSTAL STRUCTURE AND METHODS

The compounds $Ce_3A_4M_3$ ($A = Bi, Sb, M = Pt, Pd$) are a family of cubic intermetallics that crystallize in the body-centred $Y_3Sb_4Au_3$ structure [25] which has the nonsymmorphic space-group $I-43d$, two formula units per unit cell and a lattice constant $a = 10.051\text{--}10.058$ Å [7–9,12] ($a = 9.814$ Å [26]) for $Ce_3Bi_4Pt_3$ and $Ce_3Bi_4Pd_3$ ($Ce_3Sb_4Pt_3$). In our band-structure calculations we used $a = 10.051$ Å ($a = 9.814$ Å) for $Ce_3Bi_4M_3$ ($Ce_3Sb_4M_3$), as motivated below in Sec. IV A. In all four compounds, the Ce atoms occupy in Wyckoff position $12a$ ($\frac{3}{8}, 0, \frac{1}{4}$), Pt/Pd sits at site $12b$ ($\frac{7}{8}, 0, \frac{1}{4}$), and Bi/Sb is found at (u, u, u) . Here, we have followed Ref. [27] and used the ideal position $u = \frac{1}{12}$, which is very close to $u = 0.0857$ found for $Ce_3Bi_4Pt_3$ [8] and $u = 0.084$ of $Ce_3Bi_4Pd_3$ [9].

In this setting, we performed density functional theory (DFT) calculations using the WIEN2K package [28]. Unless otherwise noted, we employed the PBE functional, and

included spin-orbit coupling (SOC) in the scalar relativistic approximation for all atoms. Volume optimizations were performed with 12^3 reducible k points, self-consistency for experimental lattice constants was reached with a k mesh of 20^3 points. We use the auxiliary Kohn-Sham spectrum as proxy for the electronic structure of the studied materials. Statements about interatomic hybridizations are based on (a) maximally localized Wannier functions [29] constructed in the total angular momentum J basis for the subspace of Ce- $4f$, A- p , and M- d orbitals with WANNIER90 [30] via WIEN2WANNIER [31] and using a tool of Fernandez Afonso [32] to rotate the local spin coordinate system; (b) a local projection formalism due to Haule *et al.* [33]. The investigation of the electronic structure of the Pt members has been pioneered by Takegahara *et al.* [27]. The band structures and density of states of the two Bi compounds have been previously shown in the review article [4].

Comment: Band theory for Kondo insulators

Given that effective one-particle theories fail in most respects for systems with f electrons, a few comments are in order. Indeed, the presence of quasilocated states makes the use of genuine many-body methods a prerequisite for an adequate description (see, e.g., Refs. [14,16,33–41]). Nonetheless, conventional electronic structure theory can give meaningful insights into at least the trends of properties in families of f -electron compounds [6,42,43].

This is particularly true for (Ce-based) Kondo insulators: In the language of the Kondo lattice model (KLM), the charge gap in Kondo insulators is interaction driven through the Kondo coupling J_K . However, this spin-fermion interaction is not a fundamental force, but a quantity that emerges in the renormalization-group-like flow to a low-energy description. Indeed, it is well known that the KLM can be obtained as a limiting case of the periodic Anderson model (PAM), which contains the Hubbard U interaction as a remnant of the fundamental Coulomb force: the strong U -coupling limit of the PAM yields the weak J_K -coupling regime of the KLM with $J_K \propto V^2/U$.¹ The above illustrates that (bare) hybridizations V between conduction electrons and the f level and the Hubbard interaction U , together, generate the Kondo coupling. Note that, while the KLM is metallic for vanishing interaction, $J_K = 0$, in the absence of Hubbard U interactions, the (symmetric, half-filled) PAM is a band insulator with a gap $\Delta = 2V$. In this sense, the Kondo insulating gap in the PAM is not interaction driven. Similarly, band theory finds $\text{Ce}_3\text{A}_4\text{M}_3$ to be covalent band insulators. Band theory of course grossly overestimates the hybridization V of the $4f$ states with their surroundings and hence the band gap, both of which will get renormalized through many-body effects. Yet, the bare (DFT) band gap is directly sensitive to changes in the lanthanide environment (external pressure, isoelectronic substitutions) and can therefore qualitatively capture modifications in the essential interatomic hybridizations. Hence, *trends* in the hybridization gap of $\text{Ce}_3\text{A}_4\text{M}_3$ within band theory can be used as a gauge for the (one-particle ingredient to

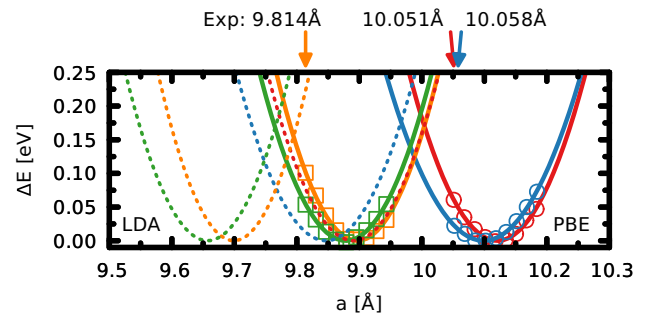


FIG. 3. Experimental and theoretical lattice constants. Shown is the relative energy difference ΔE for varying lattice constant a , using the PBE (symbols and solid lines) and the LDA (dashed lines) potential, where lines are parabolic fits. Arrows indicate experimental lattice constants (see text). The colors are chosen as follows: $\text{Ce}_3\text{Bi}_4\text{Pt}_3$ (red), $\text{Ce}_3\text{Bi}_4\text{Pd}_3$ (blue), $\text{Ce}_3\text{Sb}_4\text{Pt}_3$ (yellow), $\text{Ce}_3\text{Sb}_4\text{Pd}_3$ (green). In that order, the computed equilibrium lattice constants are 10.12, 10.10, 9.90, and 9.88 Å with PBE and 9.89, 9.85, 9.70, and 9.66 Å using LDA.

the) Kondo coupling. As a secondary effect, also the Hubbard U can potentially change through modifications in screening strengths and the localization of orbitals. Our comparison here implicitly assumes these effects to be subleading. As of now, little is known from first principles about trends in the Hubbard U in systems as complex as those considered here. Using additional information from experiment, this uncertainty can be circumvented and interaction effects assessed. This will be done in Sec. IV D.

Let us note factors that facilitate the relevance of band theory in the current case: (i) the nominal configuration in Ce-based compounds is $4f^1$ [44–46]; therefore, multiplet effects are less crucial than in systems with more electrons in the f shell;² (ii) the f electrons in Ce materials are more delocalized than, e.g., in the hole analogs based on trivalent Yb; (iii) contrary to Mott insulators, the self-energy of Kondo insulators is benign near the Fermi level [4], yielding a renormalized band structure below the Kondo temperature.

IV. RESULTS AND DISCUSSION

A. Volume optimization

We assess the isovolume nature of $\text{Ce}_3\text{Bi}_4(\text{Pt}_{1-x}\text{Pd}_x)_3$ by optimizing the volume of the end members ($x = 0, 1$) within DFT for fixed fractional atomic positions. As can be seen in Fig. 3 the theoretical lattice constants of $\text{Ce}_3\text{Bi}_4\text{Pt}_3$ and $\text{Ce}_3\text{Bi}_4\text{Pd}_3$, identified as the minima in the energy curves, are indeed very similar. We find, using PBE and the Pt compound as reference, $\Delta a/a = 0.2\%$. Experiments find instead that $\text{Ce}_3\text{Bi}_4\text{Pd}_3$ is minutely larger than $\text{Ce}_3\text{Bi}_4\text{Pt}_3$: $\Delta a/a = -0.07\%$ [12]. We repeat the same calculations for the pair $\text{Ce}_3\text{Sb}_4\text{M}_3$ ($M = \text{Pt}, \text{Pd}$). We find that exchanging Bi with Sb yields significantly smaller compounds. Crucially, however, the exchange $\text{Pt} \leftrightarrow \text{Pd}$ leads again only to very small changes:

¹Actually, there exists an exact mapping of the PAM to the KLM beyond the Kondo regime [68].

²See, however, e.g., Refs. [37,69] for multiplet effects in Ce compounds under external pressure.

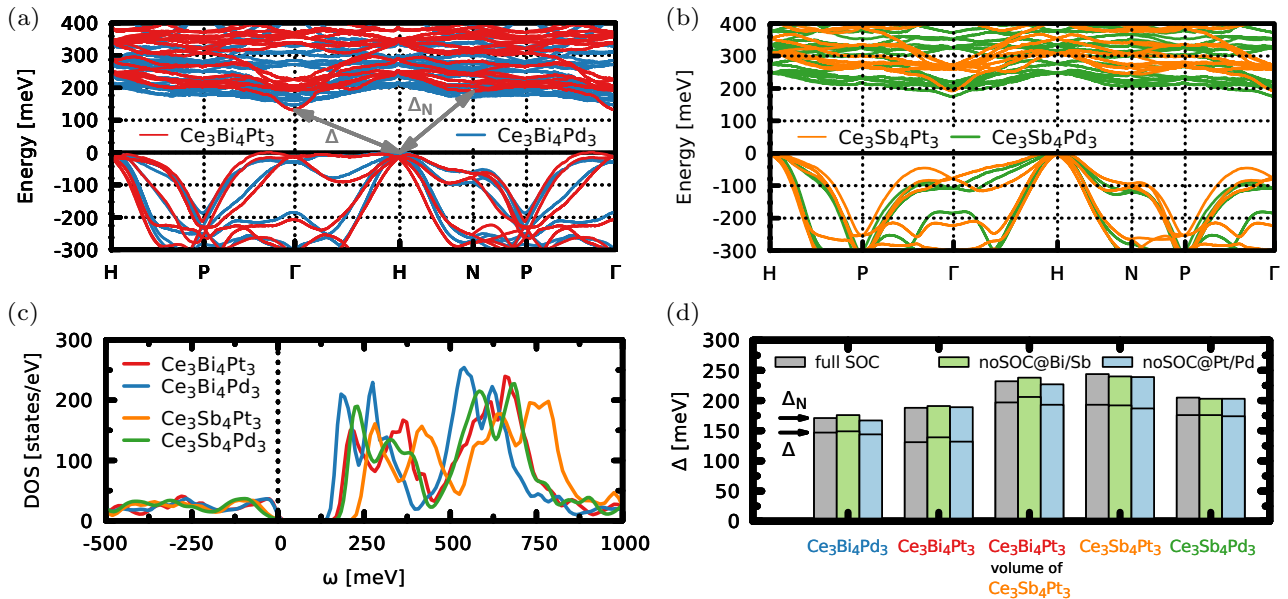


FIG. 4. Band-theory results. Band structures of (a) $\text{Ce}_3\text{Bi}_4\text{Pt}_3$ and $\text{Ce}_3\text{Bi}_4\text{Pd}_3$, (b) $\text{Ce}_3\text{Sb}_4\text{Pt}_3$ and $\text{Ce}_3\text{Sb}_4\text{Pd}_3$. The gray arrows in (a) indicate the fundamental indirect gap Δ and the gap Δ_N used as a proxy for the apparent gap in the density of states (DOS) shown, for all materials, in (c). (d) Charge gaps: fundamental indirect gap Δ and Δ_N as defined in (a). Selectively turning off the spin-orbit coupling (SOC) for the pnictogen and precious-metal atoms demonstrates that within DFT the SOC does not control the overall trends within this family of compounds. Additionally shown are gap values of fictitious $\text{Ce}_3\text{Bi}_4\text{Pt}_3$ that use the lattice constant/volume of $\text{Ce}_3\text{Sb}_4\text{Pt}_3$.

$\Delta a/a = 0.2\%$.³ We interpret the overall small changes in lattice constant, incurred upon precious-metal substitution, to warrant the label “isovolume.” For $\text{Ce}_3\text{Bi}_4M_3$ this supports previous experimental findings [7–9,12], while the isovolume nature of $\text{Ce}_3\text{Sb}_4(\text{Pt}_{1-x}\text{Pd}_x)_3$ is a prediction.⁴

We note the following: that replacing Pt with Pd does not affect the lattice constant is not a generic behavior. Indeed, the difference in lattice constant between CePtSn [47] and CePdSn [48], amounting to $\Delta a/a = 0.8\%$, is experimentally an order of magnitude larger than in $\text{Ce}_3\text{Bi}_4(\text{Pt}_{1-x}\text{Pd}_x)_3$. We can speculate that in the more complex unit cell of $\text{Ce}_3A_4M_3$ (in which, e.g., every “ M ” has four nearest “ A ” neighbors) small atomic differences can be better compensated than in $\text{Ce}M\text{B}$ (where each M has only three neighboring B).

We further note that, in line with common experience, PBE (LDA) overestimates (underestimates) the lattice constant. In the following electronic structure calculations we have therefore settled to employing experimental values: we use the lattice constant of $\text{Ce}_3\text{Bi}_4\text{Pt}_3$ for $\text{Ce}_3\text{Bi}_4M_3$, and the one of $\text{Ce}_3\text{Sb}_4\text{Pt}_3$ for $\text{Ce}_3\text{Sb}_4M_3$, where $M = \text{Pt}, \text{Pd}$.

B. Band structures

Figures 4(a) and 4(b) display the band structures of all $\text{Ce}_3A_4M_3$ compounds considered here, while Fig. 4(c) shows the corresponding density of states (DOS). For a given pnictogen

“ A ,” the valence states are rather similar, irrespective of the precious metal “ M .” Changing the pnictogen, results in perceptible changes of the valence states, in particular near the Brillouin zone center. Overall, the valence states are, congruent with photoemission spectroscopy [49,50], comparatively dispersive as they are dominantly of pd character. Indeed, as expected with only one nominal $4f$ electron, quasiautomatic narrow bands are prevalent only above the Fermi level, where also the DOS exhibits pronounced peaks.

In this work, we are mostly interested in the trends of the charge gap under isovalent substitutions. The gaps Δ extracted from the band structures are reported in Fig. 4(d). All gaps are indirect and spread, for most compounds, from around the H point to the zone center Γ . An exception is $\text{Ce}_3\text{Bi}_4\text{Pt}_3$, where the top of the valence bands emerges between the P and the Γ points. Another speciality of $\text{Ce}_3\text{Bi}_4\text{Pt}_3$ is the fact that the Γ -point conduction-band minimum is particularly pronounced. While the DOS, dominated by the f spectral weight, suggests that the charge gap *increases* when substituting Pd for Pt, the fundamental gap of $\text{Ce}_3\text{Bi}_4\text{Pd}_3$ (controlled by a dispersive band dipping down through the flat $4f$ bands at Γ) is actually larger than in $\text{Ce}_3\text{Bi}_4\text{Pt}_3$ within DFT. Since we believe the physics of these compounds to be dominated by the f electrons, we introduce (as a proxy for the trends in the f -band position) the quantity Δ_N which measures the gap between the Fermi level and onset of the conduction states at the N point. To disentangle putative control parameters of the charge gap, we report in Fig. 4(d) also the values of Δ and Δ_N when turning off the SOC on selected atoms. Furthermore, so as to demonstrate the effect of the unit-cell volume onto the charge gap, we also show results for a fictitious variant of $\text{Ce}_3\text{Bi}_4\text{Pt}_3$ that has the lattice constant of $\text{Ce}_3\text{Sb}_4\text{Pt}_3$.

³All relative changes are slightly larger when using the local density approximation (LDA) instead of PBE.

⁴While we only study the end-member compounds, the volumetric trend along the series will be, according to Vegard’s law, an interpolation between them.

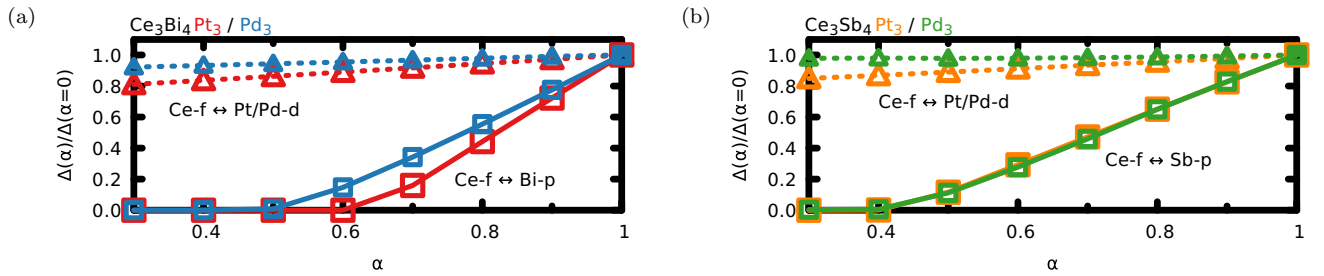


FIG. 5. Hybridization nature of the charge gap. Shown is the relative magnitude of the gap Δ when scaling the hybridization between the Ce-4*f* and the *M-d* (*M* = Pt, Pd) or *A-p* (*A* = Bi, Sb) orbitals in a maximally localized Wannier basis with a factor $\alpha \leq 1$ for (a) $\text{Ce}_3\text{Bi}_4\text{M}_3$ and (b) $\text{Ce}_3\text{Sb}_4\text{M}_3$.

C. Analysis of electronic structure

In this discussion section, we assess the influence of the spin-orbit coupling, the unit-cell volume, and the radial extent of orbitals onto the charge gap.

1. Spin-orbit coupling

As seen in Fig. 4(d), the SOC is, within DFT, irrelevant for the qualitative trends of the charge gap in this family of compounds: Turning selectively off the SOC for Pt in $\text{Ce}_3\text{Bi}_4\text{Pt}_3$ (to simulate the change in atomic mass of the precious-metal atoms) does *not* result in a band gap comparable to isovolume $\text{Ce}_3\text{Bi}_4\text{Pd}_3$. In fact, this procedure yields a Δ and Δ_N that surpass the values obtained with SOC on all atoms. Hence, the difference in masses of Pt and Pd and the resulting change in the magnitude of relativistic effects is likely not the driver of the Kondo insulator to semimetal transition in $\text{Ce}_3\text{Bi}_4(\text{Pt}_{1-x}\text{Pd}_x)_3$ of Ref. [12] (see also the discussion in Ref. [4]). Also, eliminating the SOC of Bi in $\text{Ce}_3\text{Bi}_4\text{Pt}_3$ (to simulate a smaller pnictogen mass when going to $\text{Ce}_3\text{Sb}_4\text{Pt}_3$) cannot bridge the disparity of band gaps in these two materials. The spin-orbit coupling propels the properties neither along the vertical (Bi \leftrightarrow Sb) nor the horizontal (Pt \leftrightarrow Pd) arrow in Fig. 1.

2. Hybridization nature of the gap

A far more common tuning parameter in heavy fermion systems is the unit-cell volume. While the precious-metal substitution series $\text{Ce}_3\text{Bi}_4(\text{Pt}_{1-x}\text{Pd}_x)_3$ is isovolume [7–9,12], changing the pnictogen atom from Bi to Sb decreases the lattice constant by 2% [7,8,26]. To isolate the effect of the lattice, we report, in Fig. 4(d), the charge gap of fictitious $\text{Ce}_3\text{Bi}_4\text{Pt}_3$ where the lattice constant has been artificially shrunken to the value realized in $\text{Ce}_3\text{Sb}_4\text{Pt}_3$. With respect to true $\text{Ce}_3\text{Bi}_4\text{Pt}_3$, we find a significantly increased gap. In fact, the change in the unit-cell volume accounts for almost 80% of the gap difference between $\text{Ce}_3\text{Sb}_4\text{Pt}_3$ and $\text{Ce}_3\text{Bi}_4\text{Pt}_3$. This finding identifies the unit-cell volume as the leading protagonist for the trends between the Bi and the Sb *pairs* of materials.

That the lattice has such a large effect onto the electronic structure finds its origin in the hybridization nature of the gap in these systems. Indeed, as has been demonstrated in Ref. [4], it is the hybridization of the Ce-4*f* orbitals to their surrounding that accounts for the gap opening: Treating the Ce-*f* ($J = \frac{5}{2}$) as core states results in metallic ground states,

in analogy to a periodic Anderson model with vanishing hybridization between localized *f* and conduction states.

Here, we want to further distinguish the individual contributions of atoms/orbitals to the hybridization gap Δ . To this end, we constructed maximally localized Wannier functions (see Sec. III) and expressed the projected DFT Hamiltonian in that basis. Figure 5 shows what happens to the relative magnitude of the gap in (a) $\text{Ce}_3\text{Bi}_4\text{M}_3$ and (b) $\text{Ce}_3\text{Sb}_4\text{M}_3$ when the hybridization (off-diagonal elements in the Hamiltonian) between the Ce-4*f* orbitals and the *M-d* (*M* = Pt, Pd) or the Bi/Sb-*p* orbitals is scaled with a factor $\alpha \leq 1$.⁵ We find the gap to be most sensitive to changes in the hybridization between the 4*f* orbitals of Ce and the *p* orbitals of Bi and Sb. For the Sb compounds, a smaller scaling factor α is needed to collapse the gap, congruent with $\text{Ce}_3\text{Sb}_4\text{M}_3$ having larger hybridizations than their Bi counterparts. The gap is much less sensitive to hybridizations between the Ce-*f* and the precious-metal *M-d* orbitals. We note that for both *A* = Bi and *A* = Sb the gap is more quickly diminished with α if the precious metal is *M* = Pt. The relative suppression of $\Delta(\alpha)$ when scaling the precious-metal hybridization is similar irrespective of the type of the pnictogen *A*. This finding supports the assertion that the anticipated diminishing of the gap in $\text{Ce}_3\text{Sb}_4(\text{Pt}_{1-x}\text{Pd}_x)_3$ with *x* is not volume driven, akin to what happens in $\text{Ce}_3\text{Bi}_4(\text{Pt}_{1-x}\text{Pd}_x)_3$.

3. Radial extent of orbitals

Now we will disentangle changes in the interatomic hybridization mediated by (i) the unit-cell volume and (ii) the radial extent of pertinent orbitals. To this end, we analyze the orbitally (*l*)-resolved spread $\Omega_l = \langle |R|^2 |l\rangle - \langle |R| |l\rangle^2$ of the Wannier functions, the sum of which is minimized in the maximally localization procedure [29]. We define the mean extent of a type *L* of orbitals as the average of the square root of the *l*-resolved Wannier spread: $\bar{R}_L = 1/N_L \sum_{l \in L} \sqrt{\Omega_l}$. For example, in case of the Ce-4*f* orbitals, i.e., *L* = 4*f*, *l* runs over the $N_L = 14$ spin orbitals per Ce atom. Figure 6 visualizes the thus measured size of orbitals to scale with nearest-neighbor atomic distances for (a) $\text{Ce}_3\text{Bi}_4\text{M}_3$, (b) $\text{Ce}_3\text{Sb}_4\text{M}_3$ where *M* = Pt, Pd. Figure 6(c) displays the trends of \bar{R}_L for precious-metal and pnictogen substitutions relative to the materials' lattice constant *a*.

⁵See also Ref. [4] where such a construction helped distinguishing the gap nature in covalent FeSi and ionic LaCoO₃.

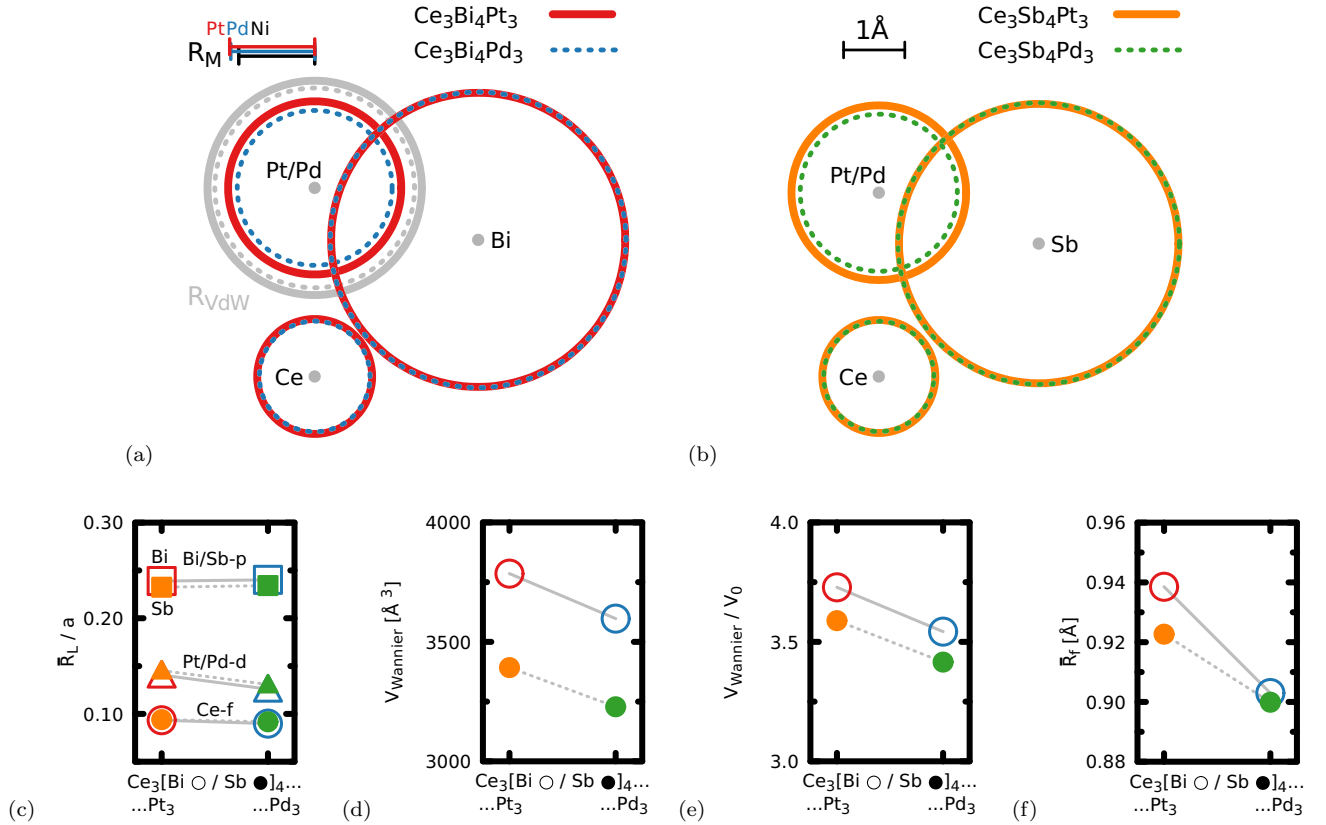


FIG. 6. The radial extent of orbitals. (a), (b) Visualize (to scale) the average radial extent (square root of the Wannier spread) of the Ce- f , M - d ($M = \text{Pt}, \text{Pd}$), A - p ($A = \text{Bi}, \text{Sb}$) orbitals in relation to interatomic nearest-neighbor distances. Also shown in (a) is the van der Waals radius R_{vdW} of Pt (1.75 Å) and Pd (1.63 Å) [51] in solid (dashed) gray, as well as the metallic radii R_M of Pt (1.39 Å), Pd (1.37 Å), and Ni (1.24 Å) [52]. (c) Displays the average radial extent \bar{R}_L relative to the respective lattice constant a . (d) Shows the summed volume V_{Wannier} of all Wannier orbital spheres of radius R_L in the unit cell. (e) Shows the same as (c) but divided by the unit-cell volume V_0 . (f) Displays the average radial extent \bar{R}_f of the Ce-4f orbitals; the relative extent \bar{R}_f/a is shown in Fig. 7.

First, we discuss the trends upon interchanging $\text{Pt} \leftrightarrow \text{Pd}$. Congruent with the precious metals' van der Waals [51] and metallic [52] radii indicated in Fig. 6(a), we find the Pd-4d orbitals to be smaller than the Pt-5d ones, irrespective of the pnictogen. The Bi and Sb- p orbitals instead are slightly larger when the precious metal is palladium, which in part compensates for the chemical pressure of the smaller Pd. It is thus suggestive to ascribe this expansion of the pnictogen to play a role in the $\text{Ce}_3\text{Bi}_4(\text{Pt}_{1-x}\text{Pd}_x)_3$ series being isovolume. Nonetheless, computing the volume of all “Wannier spheres” (of radii \bar{R}_L) in the unit cell, $V_{\text{Wannier}} = 4/3\pi \times (6 \times 14\bar{R}_f^3 + 8 \times 6\bar{R}_p^3 + 6 \times 10\bar{R}_d^3)$, we find for $\text{Ce}_3\text{Bi}_4\text{Pt}_3$ ($V_{\text{Wannier}} = 3786 \text{ \AA}^3$) a value still larger by 5% than for $\text{Ce}_3\text{Bi}_4\text{Pd}_3$ ($V_{\text{Wannier}} = 3597 \text{ \AA}^3$) [see Fig. 6(d)]. The relative difference is similar for the Sb-based compounds $\text{Ce}_3\text{Sb}_4\text{Pt}_3$ ($V_{\text{Wannier}} = 3392 \text{ \AA}^3$) and $\text{Ce}_3\text{Sb}_4\text{Pd}_3$ ($V_{\text{Wannier}} = 3228 \text{ \AA}^3$). This suggests that the crystal structure is held together dominantly by the (much larger) pnictogen p orbitals, while the contribution to bonding from the precious-metal d orbitals is subleading. The small dependence of the hybridization gap on the Ce-4f to Pt/Pd- d hopping (see Fig. 5) supports this statement.

The above is further substantiated when looking at the exchange of the pnictogen: $\text{Bi} \leftrightarrow \text{Sb}$. There, we find the smaller orbitals of the Sb-based compounds to be in line with the

smaller unit-cell volume as compared to their Bi counterparts [lattice constants: 10.051 Å for $\text{Ce}_3\text{Bi}_4M_3$ and 9.814 Å for $\text{Ce}_3\text{Sb}_4\text{Pt}_3$ (see Sec. IV A)]. Indeed, the Wannier volume (as defined above) decreases by more than 10% when replacing Bi with Sb [see Fig. 6(d)]. Note that this trend with (pnictogen) chemical pressure is opposite to the generic behavior of Wannier functions under external pressure, where the spread increases when the volume shrinks [53,54]. When rescaling V_{Wannier} with the unit-cell volume $V_0 = a^3$ [see Fig. 6(e)], we find the relative differences between the pairs with fixed precious metal M to more than halve. Hence, for the $\text{Bi} \leftrightarrow \text{Sb}$ substitution, the intuitive correspondence between the size of (p) orbitals that mediate bonding and the resulting lattice constant holds to a large extent.

Finally, we discuss the extent of the Ce-4f orbitals. The differences in \bar{R}_f between the four compounds may seem minute on the scale of Figs. 6(a)–6(c), yet their trends are revealing [see Fig. 6(f)]: Indeed, while for a given precious metal, a swapping of the pnictogen does not change the size of the 4f shell by much, replacing the precious-metal Pt with Pd significantly decreasing \bar{R}_f despite leaving the unit-cell volume inert. This suggests that, for the chosen compounds, the impact of (i) the unit-cell volume and (ii) the relative extent of the 4f orbitals can be approximately disentangled.

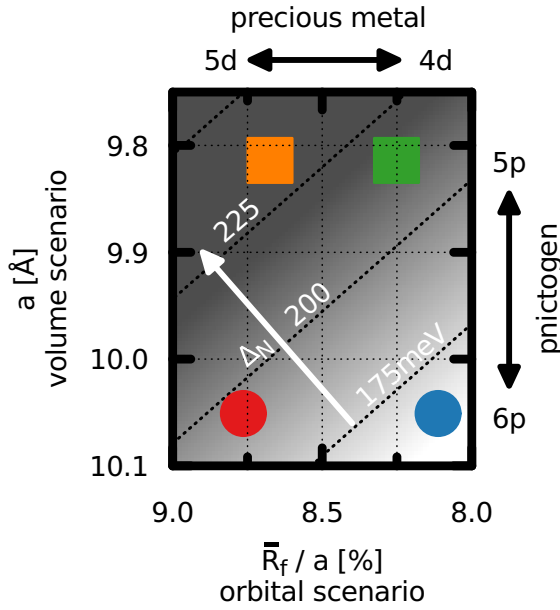


FIG. 7. Control parameters. The figure shows a (linearly interpolated) intensity map of the charge gap Δ_N of $\text{Ce}_3\text{Bi}_4\text{Pt}_3$ (red), $\text{Ce}_3\text{Bi}_4\text{Pd}_3$ (blue), $\text{Ce}_3\text{Sb}_4\text{Pt}_3$ (yellow), and $\text{Ce}_3\text{Sb}_4\text{Pd}_3$ (green) as a function of the lattice constant a and the relative extent \bar{R}_f/a of the Ce-4*f* orbitals. The substitution of the precious-metal Pt \leftrightarrow Pd (horizontal arrow) only changes the size of the orbitals, while the pnictogen replacement Bi \leftrightarrow Sb (vertical arrow) dominantly engages the unit-cell volume.

Figure 7 visualizes this central result: The charge gap of our four compounds can be well characterized as a function of their lattice constant a and the relative extent \bar{R}_f/a of their *f* orbitals, $\Delta_N = \Delta_N(a, \bar{R}_f/a)$. Quite intuitively, Δ_N increases with shrinking volume and larger relative orbital extent, as both lead to larger orbital overlaps/hybridizations. Most importantly, from this representation it is apparent that the isoelectronic pnictogen replacement primarily acts on the lattice constant, while the relative extent of the *f* shell is well-nigh untouched. The isoelectronic tuning mediated by an exchange of the precious metal, on the other hand, leaves the volume fixed, but expands or shrinks the *f* orbitals' reach relative to the surrounding atoms.

We have thus identified a viable choice of essentially *independent* variables that connect our four materials in parameter space: Fig. 7 mirrors Fig. 1 in a one-to-one fashion (if rotated by 40° to the right).

D. Anticipated many-body renormalizations

Having discussed the one-particle ingredients to the $\text{Ce}_3\text{A}_4\text{M}_3$ compounds, we now estimate the impact of many-particle interactions. For this, we transition to a more many-body oriented language: In the spirit of the Anderson impurity model, the embedding of the correlated Ce-4*f* orbitals into the solid is often described by a so-called hybridization function $\Delta(\omega) = \omega + \mu - H_{ff}^{\text{loc}} - (G_{\text{loc}}^{-1})_{ff}$. Here, μ is the chemical potential, and H^{loc} and G_{loc} are the local projections [33] of the Hamiltonian and the Green's function, respectively, while the subscripts *f* denote the evaluation within the *f*-orbital

TABLE I. Collection of experimental T_χ^{max} (see Fig. 2), estimated Kondo temperatures $T_K = 4T_\chi^{\text{max}}/(2J + 1)$ with $J = \frac{5}{2}$, m_J -averaged peak magnitude of the hybridization function $-\text{Im}\Delta(\omega_{\text{max}})$, and anticipated mass renormalization $1/Z$ estimated via $k_B T_K = -(\pi/4)\text{Im}\Delta(\omega_{\text{max}}) \times Z/(2J + 1)$; the gap Δ is estimated via $Z \times \Delta_{\text{DFT}}$. Experimental values for $\text{Ce}_3\text{Sb}_4\text{Pd}_3$ have yet to be determined (and are indicated by question marks).

Material	Expt.		Theory	Prediction	
	T_χ^{max} (K)	T_K (K)	$\langle -\text{Im}\Delta(\omega_{\text{max}}) \rangle_{m_J}$ (meV)	$m^*/m_{\text{band}} = 1/Z$	Δ (meV)
$\text{Ce}_3\text{Bi}_4\text{Pt}_3$	80	53	400	11	17
$\text{Ce}_3\text{Bi}_4\text{Pd}_3$	10	7	290	66	2.6
$\text{Ce}_3\text{Sb}_4\text{Pt}_3$	400	265	480	2.7	90
$\text{Ce}_3\text{Sb}_4\text{Pd}_3$?	?	300	?	?

subspace. Indeed, $\Delta(\omega)$ is the backbone of dynamical mean-field theory (DMFT) [55], where it is promoted to a self-consistent Weiss field. However, already on the level of DFT, the hybridization function can divulge important physical insight, in particular regarding *trends* among material families [6,43]. Moreover, $\Delta(\omega)$ can be used to classify insulators [14], e.g., distinguishing between Mott and Kondo insulators.

For our four materials, Fig. 8(a) displays the imaginary parts of the DFT hybridization function, while Fig. 8(b) shows the corresponding positions ω_{max} and peak amplitudes $-\text{Im}\Delta(\omega_{\text{max}})$. In both cases, the origin of energy corresponds to the top of the valence bands, and we have limited the presentation to the $m_J = \frac{1}{2}$ and $\frac{5}{2}$ components of the $J = \frac{5}{2}$ multiplet (the $m_J = \frac{3}{2}$ components are the smallest).

Overall, the Bi compounds exhibit peaks that are sharper and nearer to the Fermi level, indicating that these materials are closer to the flat-band limit. In the latter, an *f*-level hybridizes with a dispersionless conduction band, yielding $-\text{Im}\Delta(\omega) = \pi V^2 \delta(\omega + \mu - \omega_{\text{max}})$, where $V_{\mathbf{k}} = V$ is the amplitude of the hybridization between the conduction band and the Ce-4*f* orbitals and $\epsilon_{\mathbf{k}} = \omega_{\text{max}}$ the position of the conduction band. For conduction states $\epsilon_{\mathbf{k}}$ and couplings $V_{\mathbf{k}}$ with finite momentum dependence, the hybridization strength is spread over larger energies. The latter is the case for the Sb members of the $\text{Ce}_3\text{A}_4\text{M}_3$ family. For a given pnictogen *A*, the hybridization function is much more pronounced for Pt than for Pd, as could be anticipated from the size of orbitals (5*d* vs 4*d*) as discussed in the previous section.

Using the DFT hybridization function in conjunction with the experimental magnetic susceptibility, we can estimate the magnitude of many-body renormalizations (see Table I). We use two complementary formulas for the Kondo temperature: First, we assess T_K from the spin degrees of freedom using the Kondo lattice expression $T_K = 4T_\chi^{\text{max}}/(2J + 1)$ [56] with $J = \frac{5}{2}$ and T_χ^{max} (the temperature where the magnetic susceptibility peaks) is extracted from experiment (see Fig. 2). Note that the estimate of T_K of $\text{Ce}_3\text{Bi}_4\text{Pd}_3$ is of the same order of magnitude of what has been deduced from the experimental specific heat [12]. Second, the Kondo temperature is determined from the charge degrees of freedom: $k_B T_K = -(\pi/4)\text{Im}\Delta(\omega_{\text{max}}) \times Z/(2J + 1)$ [56,57]. With the T_K from above, we then solve for the effective mass enhancement $1/Z$.

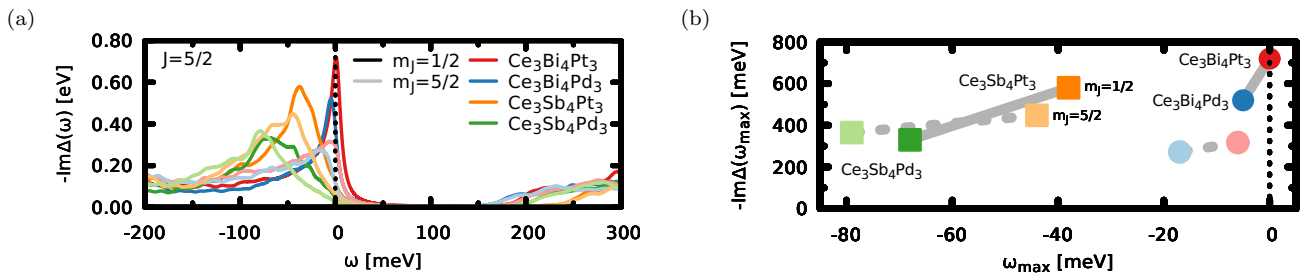


FIG. 8. Hybridization function $\Delta(\omega)$. (a) Shows the imaginary part of the DFT hybridization function $\Delta(\omega)$, resolved into its m_J components. (b) Indicates the trends in the maximal amplitude of the $m_J = \frac{1}{2}$ component of $\Delta(\omega)$ and the frequency ω_{\max} where the latter occurs. The origin of energy corresponds to the valence-band maximum.

For $\text{Ce}_3\text{Bi}_4\text{Pt}_3$, we find $Z \approx \frac{1}{10}$, in excellent agreement with recent realistic DMFT calculations [14]. While for the other compounds, a quantitative theoretical assessment has to await the application of many-body electronic structure methods [55,58],⁶ we believe the following simple estimates to reflect at least the *hierarchy* of effective masses in the $\text{Ce}_3\text{A}_4\text{M}_3$ family: The largely reduced Kondo temperature when substituting Pd for Pt accounts for $\text{Ce}_3\text{Bi}_4\text{Pd}_3$ having the largest effective mass ($1/Z = 66$), as well as for $\text{Ce}_3\text{Sb}_4\text{Pt}_3$ being less correlated than $\text{Ce}_3\text{Bi}_4\text{Pt}_3$. Naively applying the mass renormalization of $\text{Ce}_3\text{Bi}_4\text{Pd}_3$ to its DFT band gap⁷ yields 2.6 meV, in good agreement with an experimental estimate of 1.8 ± 0.5 meV [17]. Doing the same for $\text{Ce}_3\text{Sb}_4\text{Pt}_3$, however, significantly overestimates the gap. We can surmise that the Sb compounds are further from a description in terms of fully localized f states, which renders the Kondo lattice formula used in the determination of T_K less reliable.

Given the trends in the band gaps, hybridization functions, and the Kondo temperature (that itself depends on the two former), we nonetheless gauge the $\text{Ce}_3\text{Sb}_4\text{Pd}_3$ compound, that we propose experimentalists to synthesize, to exhibit mass enhancements of the order of 10.

E. Isoelectronic tuning: A perspective

Let us put our findings into perspective: The Kondo coupling in f -electron materials can be dramatically affected by (i) pressure or by (ii) isoelectronic substitutions with atoms of varying size [2]. Here, we have demonstrated that these two routes can be *linearly independent*. Aside from the effect of exercising chemical pressure, the change in the principal quantum number n of substituted atoms, e.g., Pt: $n = 5$, Pd: $n = 4$, may largely change the charge gap while having little or no effect on cohesive properties. The isoelectronic tuning scenario that we propose extends the empirical volume picture (valid in binary compounds) to include orbital effects at constant volume. In this regard, the $\text{Ce}_3\text{A}_4\text{M}_3$ system is an ideal case, in that the changes in the lattice constant induced by different A atoms and the relative orbital extent of M atoms form an essentially orthogonal coordinate system. In

general, volume and \bar{R}_f/a will provide linear independent yet skewed coordinates. Near orthogonality of these control parameters is likely realized for replacements of atoms (like $\text{Pt} \leftrightarrow \text{Pd}$) that have comparable electronegativities and (empirical, van der Waals, or metallic) atomic radii (see below for a “nonorthogonal” example). It also stands to reason that an isovolume tuning of interatomic hybridizations, and hence the Kondo coupling, is more prevalent in complex materials (ternary compounds and above) and for substitutions of atoms that contribute only subleadingly to the charge gap/bonding [as is the case for the precious metal M in $\text{Ce}_3\text{A}_4\text{M}_3$ (cf. Fig. 5 and the discussion above)].

The proposed interperiod orbital scenario will be relevant to other heavy fermion systems. A putative example is the $\text{Ce}(\text{Ni},\text{Pd})\text{Sn}$ system: CePdSn is an antiferromagnetic Kondo metal with a Néel temperature of about 7 K [48,59,60], while CeNiSn is a paramagnetic anisotropic Kondo insulator [61,62]. In the standard Doniach phase diagram [5], CePdSn falls into the regime dominated by the Ruderman-Kittel-Kasuya-Yosida interaction, whereas CeNiSn realizes a larger Kondo coupling J_K that impedes long-range magnetic order. This interpretation is congruent with the “volume scenario”: CeNiSn has a unit-cell volume (263.6 \AA^3) smaller by 6% than CePdSn (281.7 \AA^3) [60] arguably leading to larger hybridizations and, hence, bigger J_K . However, it has been highlighted [2] that there is a significant difference between the isoelectronic substitution series, $\text{Ce}(\text{Pd}_{1-x}\text{Ni}_x)\text{Sn}$, that connects the two compounds, and CePdSn under hydrostatic pressure. Indeed, while the Néel temperature is fully suppressed for $x \geq 0.75$ [63], the pressure needed to achieve the same is at least 6 GPa [60], which, using the bulk modulus 55.6 GPa of CeNiSn [64], corresponds to a volume reduction of more than 10%: an *external* compression of almost twice as much is required to equal the effect of *chemical* pressure. With the “orbital scenario” proposed above, this large quantitative discrepancy is readily explained: As suggested by the metallic radii R_M of Pd and Ni [52] [both are indicated in Fig. 6(a)], the $3d$ orbitals of Ni will be smaller than the $4d$ of Pd. We therefore hypothesize that for growing x in $\text{CeNi}_x\text{Pd}_{1-x}\text{Sn}$ the shrinking of the unit-cell volume and the decrease of the orbital extent conspire to jointly reduce the Kondo coupling, driving the system faster toward smaller J_K coupling in the Doniach phase diagram.⁸ The scenario might also be of

⁶For the temperature dependence of $\Delta(\omega)$ in $\text{Ce}_3\text{Bi}_4\text{Pt}_3$, see Ref. [14]; for spectral properties of $\text{Ce}_3\text{Bi}_4\text{Pt}_3$ and $\text{Ce}_3\text{Bi}_4\text{Pd}_3$, see Refs. [14,16].

⁷That is, neglecting potential nonlinear effects in the self-energy.

⁸Disorder in the series could further destabilize the Néel order.

relevance in the comparison of CeRu_4Sn_6 [65] under external [66,67] and chemical ($\text{Sn} \rightarrow \text{Ge}$) [67] pressure. In fact, it will be interesting to gain systematic insights into larger groups of materials to assess the described physics. Indeed, we believe that \bar{R}_f/a could be a useful quantity in databases for heavy fermion material properties [6,43]. Its approximation R_M/a , using tabulated metallic radii R_M , could even be used as descriptor in high-throughput surveys.⁹

V. CONCLUSIONS

We have shown the suppression of coherence and energy scales in isoelectronic and isovolume $\text{Ce}_3\text{Bi}_4(\text{Pt}_{1-x}\text{Pd}_x)_3$, previously attributed to changes in the spin-orbit coupling [12], to derive from a reduced Kondo coupling. The latter is tunable, even at constant volume, through the principal quantum number of orbitals that host conduction electrons. We have identified the relative extent \bar{R}_f/a of the lanthanide's f orbitals as (indirect) control parameter of the Kondo coupling and demonstrated it to be *linearly independent* from changes mediated by the unit-cell volume V_0 . In the $\text{Ce}_3\text{A}_4\text{M}_3$ system,

⁹For noncubic compounds, such as CeNiSn and CeRu_4Sn_6 , the lattice parameter a might have to be replaced with relevant nearest-neighbor distances.

the precious-metal $\text{Pt} \leftrightarrow \text{Pd}$ (pnictide $\text{Bi} \leftrightarrow \text{Sb}$) substitution only changes the f orbitals' hybridizations through \bar{R}_f/a (V_0). Our "orbital scenario" generalizes the empirical "volume scenario" (applicable to binary compounds) to isoelectronic (interperiod) tuning in complex heavy fermion materials. The two-parameter dependency $J_K = J_K(a, \bar{R}_f/a)$ may explain why there can be notable differences between external and chemical pressure, e.g., in the $\text{Ce}(\text{Ni},\text{Pd})\text{Sn}$ system.

The very small coherence scale of $\text{Ce}_3\text{Bi}_4\text{Pd}_3$ encumbers experiments. We therefore propose to synthesize the new material $\text{Ce}_3\text{Sb}_4\text{Pd}_3$. We predict it to have a unit-cell volume very close to that of $\text{Ce}_3\text{Sb}_4\text{Pt}_3$, and a mass enhancement of the order of 10. Anticipating larger gaps in $\text{Ce}_3\text{Sb}_4(\text{Pt}_{1-x}\text{Pd}_x)_3$, the series provides an attractive testing ground for our "orbital scenario" of isoelectronic tuning of energy and coherence scales.

ACKNOWLEDGMENTS

The author is indebted to J. Fernandez Afonso. Exchanges with S. Dzsaber, G. Eguchi, K. Held, J. Kuneš, S. Paschen, and Q. Si are acknowledged. This work has been supported by the Austrian Science Fund (FWF) through Project "LinReTraCe" No. P 30213-N36. The computational results presented have been achieved in part using the Vienna Scientific Cluster (VSC).

-
- [1] P. Gegenwart, Q. Si, and F. Steglich, *Nat. Phys.* **4**, 186 (2008).
 [2] Q. Si and S. Paschen, *Phys. Status Solidi B* **250**, 425 (2013).
 [3] S. Wirth and F. Steglich, *Nat. Rev. Mater.* **1**, 16051 (2016).
 [4] J. M. Tomczak, *J. Phys.: Condens. Matter* **30**, 183001 (2018).
 [5] S. Doniach, *Phys. B+C (Amsterdam)* **91**, 231 (1977).
 [6] H. C. Herper, T. Ahmed, J. M. Wills, I. Di Marco, T. Björkman, D. Iuşan, A. V. Balatsky, and O. Eriksson, *Phys. Rev. Mater.* **1**, 033802 (2017).
 [7] M. F. Hundley, P. C. Canfield, J. D. Thompson, Z. Fisk, and J. M. Lawrence, *Phys. Rev. B* **42**, 6842 (1990).
 [8] G. H. Kwei, J. M. Lawrence, P. C. Canfield, W. P. Beyermann, J. D. Thompson, Z. Fisk, A. C. Lawson, and J. A. Goldstone, *Phys. Rev. B* **46**, 8067 (1992).
 [9] W. Hermes, S. Linsinger, R. Mishra, and R. Pöttgen, *Chem. Monthly* **139**, 1143 (2008).
 [10] Z. Fisk, J. Sarrao, J. Thompson, D. Mandrus, M. Hundley, A. Miglari, B. Bucher, Z. Schlesinger, G. Aeppli, E. Bucher, J. DiTusa, C. Oglesby, H.-R. Ott, P. Canfield, and S. Brown, *Phys. B (Amsterdam)* **206-207**, 798 (1995).
 [11] P. S. Riseborough, *Adv. Phys.* **49**, 257 (2000).
 [12] S. Dzsaber, L. Prochaska, A. Sidorenko, G. Eguchi, R. Svagera, M. Waas, A. Prokofiev, Q. Si, and S. Paschen, *Phys. Rev. Lett.* **118**, 246601 (2017).
 [13] S. Dzsaber, X. Yan, G. Eguchi, A. Prokofiev, T. Shiroka, P. Blaha, O. Rubel, S. E. Grefe, H.-H. Lai, Q. Si, and S. Paschen, [arXiv:1811.02819](https://arxiv.org/abs/1811.02819).
 [14] J. M. Tomczak, [arXiv:1904.01346](https://arxiv.org/abs/1904.01346).
 [15] S. Dzsaber, D. A. Zocco, A. McCollam, F. Weickert, R. McDonald, M. Taupin, X. Yan, A. Prokofiev, L. M. K. Tang, B. Vlaar, L. Stritzinger, M. Jaime, Q. Si, and S. Paschen, [arXiv:1906.01182](https://arxiv.org/abs/1906.01182).
 [16] C. Cao, G.-X. Zhi, and J.-X. Zhu, [arXiv:1904.00675](https://arxiv.org/abs/1904.00675).
 [17] S. K. Kushwaha, M. K. Chan, J. Park, S. M. Thomas, E. D. Bauer, J. D. Thompson, F. Ronning, P. F. S. Rosa, and N. Harrison, *Nat. Commun.* **10**, 5487 (2019).
 [18] D. J. Campbell, Z. E. Brubaker, C. Roncaioli, P. Saraf, Y. Xiao, P. Chow, C. Kenney-Benson, D. Popov, R. J. Zieve, J. R. Jeffries, and J. Paglione, *Phys. Rev. B* **100**, 235133 (2019).
 [19] M. Kasaya, K. Katoh, and K. Takegahara, *Solid State Commun.* **78**, 797 (1991).
 [20] M. Kasaya, K. Katoh, M. Kohgi, T. Osakabe, and N. Sato, *Phys. B (Amsterdam)* **199-200**, 534 (1994).
 [21] C. D. W. Jones, K. A. Regan, and F. J. DiSalvo, *Phys. Rev. B* **58**, 16057 (1998).
 [22] K. Katoh and T. Takabatake, *J. Alloys Compd.* **268**, 22 (1998).
 [23] M. Dzero, J. Xia, V. Galitski, and P. Coleman, *Annu. Rev. Condens. Matter Phys.* **7**, 249 (2016).
 [24] P.-Y. Chang, O. Erten, and P. Coleman, *Nat. Phys.* **13**, 794 (2017).
 [25] A. E. Dwight, *Acta Crystallogr., Sect. B* **33**, 1579 (1977).
 [26] C. D. W. Jones, K. A. Regan, and F. J. DiSalvo, *Phys. Rev. B* **60**, 5282 (1999).
 [27] K. Takegahara, H. Harima, Y. Kaneta, and A. Yanase, *J. Phys. Soc. Jpn.* **62**, 2103 (1993).
 [28] P. Blaha, K. Schwarz, G. K. H. Madsen, D. Kvasnicka, J. Luitz, R. Laskowski, F. Tran, and L. D. Marks, *WIEN2k, An Augmented Plane Wave + Local Orbitals Program for Calculating Crystal Properties* (Karlheinz Schwarz, Techn. Universität Wien, Austria, 2018).
 [29] N. Marzari, A. A. Mostofi, J. R. Yates, I. Souza, and D. Vanderbilt, *Rev. Mod. Phys.* **84**, 1419 (2012).

- [30] A. A. Mostofi, J. R. Yates, Y.-S. Lee, I. Souza, D. Vanderbilt, and N. Marzari, *Comput. Phys. Commun.* **178**, 685 (2008).
- [31] J. Kunes, R. Arita, P. Wissgott, A. Toschi, H. Ikeda, and K. Held, *Comput. Phys. Commun.* **181**, 1888 (2010).
- [32] J. Fernandez Afonso, Excitonic condensation in strongly correlated materials, Ph.D. thesis, TU Wien, 2019.
- [33] K. Haule, C.-H. Yee, and K. Kim, *Phys. Rev. B* **81**, 195107 (2010).
- [34] K. Held, A. K. McMahan, and R. T. Scalettar, *Phys. Rev. Lett.* **87**, 276404 (2001).
- [35] B. Amadon, S. Biermann, A. Georges, and F. Aryasetiawan, *Phys. Rev. Lett.* **96**, 066402 (2006).
- [36] J. M. Tomczak, L. V. Pourovskii, L. Vaugier, A. Georges, and S. Biermann, *Proc. Natl. Acad. Sci. U. S. A.* **110**, 904 (2013).
- [37] L. V. Pourovskii, P. Hansmann, M. Ferrero, and A. Georges, *Phys. Rev. Lett.* **112**, 106407 (2014).
- [38] A. B. Shick, L. Havela, A. I. Lichtenstein, and M. I. Katsnelson, *Sci. Rep.* **5**, 15429 (2015).
- [39] P. Wissgott and K. Held, *Eur. Phys. J. B* **89**, 5 (2016).
- [40] E. Plekhanov, P. Hasnip, V. Sacksteder, M. Probert, S. J. Clark, K. Refson, and C. Weber, *Phys. Rev. B* **98**, 075129 (2018).
- [41] S. Seong, K. Kim, E. Lee, C.-J. Kang, T. Nam, B. I. Min, T. Yoshino, T. Takabatake, J. D. Denlinger, and J.-S. Kang, *Phys. Rev. B* **100**, 035121 (2019).
- [42] G. Zwicknagl, *Rep. Prog. Phys.* **79**, 124501 (2016).
- [43] H. Hafiz, A. I. Khair, H. Choi, A. Mueen, A. Bansil, S. Eidenbenz, J. Wills, J.-X. Zhu, A. V. Balatsky, and T. Ahmed, *npj Comput. Mater.* **4**, 63 (2018).
- [44] J. C. Fuggle, F. U. Hillebrecht, Z. Zolnierak, R. Lässer, C. Freiburg, O. Gunnarsson, and K. Schönhammer, *Phys. Rev. B* **27**, 7330 (1983).
- [45] F. Strigari, T. Willers, Y. Muro, K. Yutani, T. Takabatake, Z. Hu, Y.-Y. Chin, S. Agrestini, H.-J. Lin, C. T. Chen, A. Tanaka, M. W. Haverkort, L. H. Tjeng, and A. Severing, *Phys. Rev. B* **86**, 081105(R) (2012).
- [46] F. Strigari, M. Sundermann, Y. Muro, K. Yutani, T. Takabatake, K.-D. Tsuei, Y. F. Liao, A. Tanaka, P. Thalmeier, M. W. Haverkort, L. H. Tjeng, and A. Severing, *J. Electron Spectrosc. Relat. Phenom.* **199**, 56 (2015).
- [47] T. Takabatake, H. Iwasaki, G. Nakamoto, H. Fujii, H. Nakotte, F. de Boer, and V. Sechovský, *Phys. B (Amsterdam)* **183**, 108 (1993).
- [48] S. K. Malik, D. T. Adroja, S. K. Dhar, R. Vijayaraghavan, and B. D. Padalia, *Phys. Rev. B* **40**, 2414 (1989).
- [49] K. Breuer, S. Messerli, D. Purdie, M. Garnier, M. Hengsberger, G. Panaccione, Y. Baer, T. Takahashi, S. Yoshii, M. Kasaya, K. Katoh, and T. Takabatake, *Europhys. Lett.* **41**, 565 (1998).
- [50] Y. Takeda, M. Arita, H. Sato, K. Shimada, H. Namatame, M. Taniguchi, K. Katoh, F. Iga, and T. Takabatake, *J. Electron. Spectrosc.* **101-103**, 721 (1999).
- [51] A. Bondi, *J. Phys. Chem.* **68**, 441 (1964).
- [52] *Chemistry of the Elements (Second Edition)*, edited by N. Greenwood and A. Earnshaw (Butterworth-Heinemann, Oxford, 1997), pp. 1144–1172.
- [53] J. M. Tomczak, T. Miyake, R. Sakuma, and F. Aryasetiawan, *Phys. Rev. B* **79**, 235133 (2009).
- [54] J. M. Tomczak, T. Miyake, and F. Aryasetiawan, *Phys. Rev. B* **81**, 115116 (2010).
- [55] A. Georges, G. Kotliar, W. Krauth, and M. J. Rozenberg, *Rev. Mod. Phys.* **68**, 13 (1996).
- [56] P. Coleman, *Phys. Rev. B* **28**, 5255 (1983).
- [57] A. C. Hewson, *The Kondo Problem to Heavy Fermions* (Cambridge University Press, Cambridge, 1993).
- [58] J. M. Tomczak, P. Liu, A. Toschi, G. Kresse, and K. Held, *Eur. Phys. J.: Spec. Top.* **226**, 2565 (2017).
- [59] M. Kasaya, T. Tani, F. Iga, and T. Kasuya, *J. Magn. Magn. Mater.* **76-77**, 278 (1988).
- [60] F. Iga, M. Kasaya, H. Suzuki, Y. Okayama, H. Takahashi, and N. Mori, *Phys. B (Amsterdam)* **186-188**, 419 (1993).
- [61] T. Takabatake, F. Teshima, H. Fujii, S. Nishigori, T. Suzuki, T. Fujita, Y. Yamaguchi, J. Sakurai, and D. Jaccard, *Phys. Rev. B* **41**, 9607 (1990).
- [62] T. E. Mason, G. Aeppli, A. P. Ramirez, K. N. Clausen, C. Broholm, N. Stücheli, E. Bucher, and T. T. M. Palstra, *Phys. Rev. Lett.* **69**, 490 (1992).
- [63] M. Kasaya, T. Tani, H. Suzuki, K. Ohoyama, and M. Kohgi, *J. Phys. Soc. Jpn.* **60**, 2542 (1991).
- [64] K. Ikushima, H. Yasuoka, Y. Uwatoko, and Y. Isikawa, *Phys. Rev. B* **60**, 14537 (1999).
- [65] I. Das and E. V. Sampathkumaran, *Phys. Rev. B* **46**, 4250 (1992).
- [66] K. Sengupta, K. K. Iyer, R. Ranganathan, and E. V. Sampathkumaran, *J. Phys.: Conf. Ser.* **377**, 012029 (2012).
- [67] J. Zhang, S. Zhang, Z. Chen, M. Lv, H. Zhao, Y.-F. Yang, G. Chen, and P. Sun, *Chin. Phys. B* **27**, 097103 (2018).
- [68] P. Sinjukow and W. Nolting, *Phys. Rev. B* **65**, 212303 (2002).
- [69] W. M. Temmerman, A. Svane, L. Petit, M. Lüders, P. Strange, and Z. Szotek, *Phase Transitions* **80**, 415 (2007).